NUMERICAL SIMULATION OF DIFFERENT TURBULENCE MODELS AIMING AT PREDICTING THE FLOW AND TEMPERATURE SEPARATION IN A RANQUE-HILSCH VORTEX TUBE

by

Seied Hossein AZIZI [a*], Mahmoud Reza ANDALIBI [b], Seied Reza SALEH [c], and Mohsen KAHROM [d]

[a] Department of Mechanical Engineering, Bandar Lengeh Branch, Islamic Azad University, Bandar Lengeh, Iran
[b] Department of Mechanical Engineering, Bandar Lengeh Branch, Islamic Azad University, Bandar Lengeh, Iran
[c] Department of Mechanical Engineering, Mashhad Branch, Islamic Azad University, Mashhad, Iran
[d] Mechanical Engineering Department, Ferdowsi University of Mashhad, Mashhad, Iran

Original scientific paper
DOI: 10.2298/TSCI110727201A

A computational fluid dynamics model is used to compare the effect of different Reynolds averaged Navier-Stokes based turbulence models in predicting the temperature separation and power separation in a Ranque-Hilsch vortex tube. Three first order turbulence models (standard k-ε, renormalized group and shear stress transport k-ω model) together with a second order numerical scheme are surveyed in the present work. The simulations are done in 2-D steady, axisymetric with high swirl flow model. The performance curves (hot and cold outlet temperatures and power separation vs. hot outlet mass fraction) obtained by using these turbulence models are compared with the experimental results in different cold mass fractions. The aim is to select an appropriate turbulence model for the simulation of the flow phenomena. Because of large discrepancy between 2-D and experiment, validation in 3-D model is also considered. The performance analysis shows that among all the turbulence models investigated in this study, temperature separation predicted by the renormalized group model is closer to the experimental results.

Keywords: *Ranque-Hilsch vortex tube, temperature separation, power separation, k-ε model, k-ω model, RNG k-ε model*

Introduction

Vortex tube or Ranque-Hilsch tube a simple, mechanical device with no movable part can separate inlet compressed air into cold and hot temperature. The use of such device is in low temperature industrial applications including cooling machinery, cooling food, *etc*. The applicability of this device has been reported by Aronson [1] in high speed drilling mentioning a ten time life improvement of the tool. As this device has no movable part it dose not need much maintenance. Vortex measures 10-40 cm in length and is cost effective.

* Corresponding author; e-mail: s.hossein.azizi@gmail.com

Vortex tube can be classified, depending on its flow behaviour, into two types namely, the counter flow or standard vortex tube and parallel or uni-flow type. Considering counter flow vortex tube, cold and hot flows emit from the opposite ends but parallel type features same cold - hot flow exit. The device consists of a simple tube, an inlet with one or more nozzles, two outlets, and a valve adjusting the pressure and mass flow and an orifice in the cold end. High pressured air enters from the nozzles to the tube and due to the shape of nozzles it moves into azimuthal direction and makes a swirl flow with high angular velocity, followed by gas separation into hot and cold flow which is called energy or temperature separation. The hot temperature flow moves near the periphery to the hot end and the cold flow moves from core to the cold end which is near the inlet in the standard type.

This effect was first discovered by Ranque [2]. He hypothesized that the layers in the inner region expand and become cold while their pressure to the outer layers makes them grow hot, but this theory was rejected by him when he stated that the friction between the layers results in migration of energy. After Ranque a German physicist, Hilsch [3], stated that air in the cold region expands from high pressure to low pressure (near wall to core) and in this process the layers transfer some amount of their energy to the periphery region. Fulton [4] explained that the energy separation is due to the free and forced vortex generated inside the tube. The injection of gas leads to a free vortex ($V \propto r$) to form with low angular velocity near the wall and high angular velocity near the core region. The inner friction changes this free vortex into a forced one ($V \propto 1/r$) causing inner layers to lose their kinetic energy and turn cold. The energy gained from inner layers by the outer ones surpasses the energy loss near the wall leading to a higher gas temperature near the periphery Kassner and Knoernschild [5], derived the laws of shear stress from circular flow resembling theory of Fullton. They stated that the flow change from free to forced vortex is due to shear stress. In addition turbulent transport in the presence of radial pressure gradient results in temperature profile that makes the core colder than it was in forced vortex regime. Scheper [6] measured static and total temperature, pressure, velocity in a vortex tube, using probes and visualization techniques and proposed a forced heat convection theory based on his experiments. Ahlborn and Gordon [7] proposed a theory called "secondary circulation" based on his experimental results which compare the amount of mass flow near the cold region which works like a refrigeration device in a close loop and stated that this effect accounts for temperature loss in the cold region. Stephan *et al.* [8] suggested the formation of Gortler vortices near the wall of vortex tube deriving the flow motion. Gutsol [9], like Fullton, proposed a theory in which turbulent vortex motion exists in different layers and this is why the energy exchanges in vortex tube. Kurosaka [10], found a relationship between the forced vortex motion and acoustic resonance frequencies proposing that the energy separation occurs as a result of acoustic streaming damping near the axis.

Mentioned theories can be fit into following classifications: (1) Adiabatic compression and expansion, (2) Heat transfer theory, (3) Effect of friction and turbulence, (4) Acoustic streaming, and (5) Secondary circulation flow.

Most of the past works were based on theoretical studies and have unsuccessfully explained the energy separation effect in vortex tube. Some efforts have also been made based on computational fluid dynamic (CFD) to explain this effect. Frohlingsdorf and Unger [11], simulated a vortex tube numerically by using the code CFX (finite volume program) and validated their result with the experimental data presented by Bruun [12]. Promvonge [13], simulated a strong swirling compressible flow by two turbulence models in a uni-flow vortex tube to investigate its characteristics. Behera *et al*. [14] simulated a vortex tube with renormalized group

(RNG) k-ε model using Star-CD code to investigate the effect of nozzles (shape and number of nozzles) on temperature separation in a counter-flow vortex tube. Aljuwayhel *et al.* [15], used two turbulence models (k-ε and RNG k-ε) for his simulation. He divided the vortex tube in three regions, hot flow, cold flow, and re-circulating flow region to determine the rate of work and heat transfer between these regions. Skye *et al*. [16], measured the inlet and outlet temperatures experimentally and numerically with k-ε and RNG model in a commercial vortex tube. Sohn, C.-H., *et al*. [17] investigation included experimental internal flow phenomena to indicate stagnation point in a vortex tube by surface tracing method. Xue *et al*. [18] numerically studied the variation of velocity, pressure, and temperature inside a vortex tube and compared their result with the experimental data of Skye *et al*. [16] and they emphasized on the mechanism of hot peripheral flow and a reversing cold inner core flow formation. Akhesmeh *et al.* [19] discussed pressure, viscosity, turbulence, temperature, secondary circulation and acoustic streaming to present a critical review of different explanations on the working concept of a vortex tube. In order to optimize the number of nozzles of a vortex tube, Kirmaci [20] used Taguchi method in his study. Hossein Nezhad and Shamsoddini [21] also analyzed the mechanism of flow and heat transfer in a 3-D CFD model. Bramo and Pourmahmoud [22] numerical study on the effect of length to diameter ratio (L/D) revealed the occurrence of stagnation point because of its importance in flow pattern. Farouk and Farouk [23] used CFD-ACE+ code to investigate energy separation by Large eddy simulation (LES) technique comparing their result with the experimental result of Skye *et al*. [16]. They reported that temperature separation predicted by this model was more accurate than k-ε model; however, they significantly changed the diameter and inlet boundary condition of Skye's vortex tube. Dutta *et al*. [24], comparing four different turbulence model, proposed that standard k-ε model simulation was closer to the experimental result compared to, k-ε standard, RNG k-ε, and shear stress transport (SST) k-ω model. Skye *et al*. [16] also mentioned that between k-ε standard and RNG k-ε, the former can provides a more accurate prediction. On the other hand, Aljuwayhel [15] had a completely reverse idea regarding these two models.

Computation of complex flow phenomenon is a challenging task. This simulation involves high swirling compressible turbulent flow with energy separation. The present work provides a comparison of results by using three turbulence Reynolds averaged Navier-Stokes (RANS) models (k-ε standard, RNG k-ε, SST k-ω model) aiming at finding a suitable, less expensive, turbulence model. The compressible equations are numerically solved to simulate a vortex tube. The governing equations are discretized by the second order upwind scheme. Temperature separations predicted by this study are compared with the experimental and numerical k-ε results of Skye *et al*. [16]; however, due to large discrepancies between 2-D and experiment, validation in the 3-D model is also considered. More advanced turbulence models such as Reynolds stress equations, LES, and Direct numerical simulation (DNS) were investigated, but these models could not be made to converge for the present simulations.

CFD analysis of the vortex tube

The flow in vortex tube is assumed steady-state. The 2-D model is shown in fig. 1. The CFD domain in this position considered as an axis-symmetric one so only half of the domain needs to be considered, causing the calculation time to reduce. The inlet and hot exit outlets are modelled circumferentially. $V_r = 0.25V_n$, $V_\theta = 0.97V_n$. The hot exit outlet in 2-D simulation is also modelled circumferentially. The hot exit area is 95 mm^2 so the width l_h (width for outlet) can be calculated as $A_h = \pi D l_h$ and for the inlet, the equivalent width of slot is calculated from conservation of mass as was mentioned in Skye *et al*. [16].

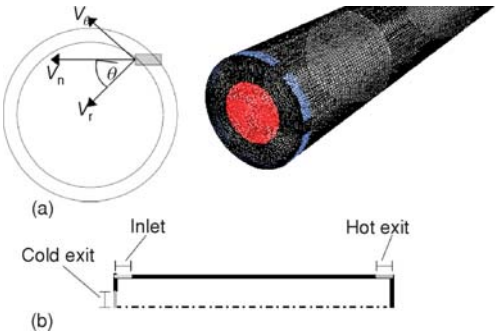

Figure 1. (a) Velocity's components direction (b) Vortex tube modelling in 2-D dimensional forms

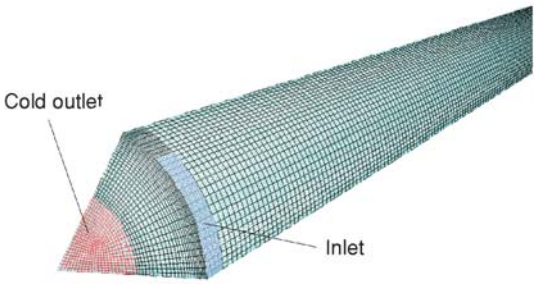

Figure 2. 3-D model of vortex tube

In 3-D domain the nozzles consists of 6 slots. The model uses a rotation periodic which means simulation of a 60° sector of flow, fig. 2.

The following assumptions should be attended for computation [16]: The gas in vortex tube is ideal, and specific heat capacity C_p is constant. The cone shaped valve used as a discharge control at the hot exit is replaced with a block valve. The dimensions are based on Skye *et al*. [16] model.

Physical modelling

An Exair 708 slpm (25 scfm) vortex tube was used to collect all the experimental data reported by Skye *et al*. [16]. Figure 3 shows that the theoretical uncertainty in the measurement (that is based on the characteristics of the instruments) as well as the measured energy balance error (which is calculated from experimental data) as a function of the cold mass fraction, follow a similar trend. Cold mass fractions with energy balance error less than 10% are used for validation of CFD results. Thus, 11 cold mass fractions were considered for validation. Table 1 provides the geometry summery of the vortex tube used for the experiment.

Grid dependence study

A grid independence study was carried out to eliminate the errors due to coarseness of grids for different average unit cell volumes. Difference between hot and cold temperature (temperature difference) as a key parameter is

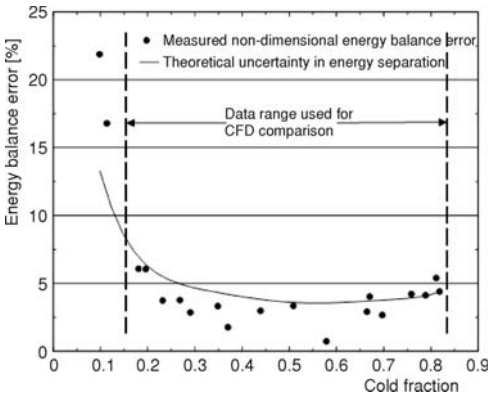

Figure 3. Theoretical uncertainty in the energy balance and the measured, non-dimensional energy balance error as a function of the cold fraction [16]

Table 1. Geometry of the experimental Skye's *et al.* vortex tube [16]

Measurement	Value
Hot exit area	95 mm^2
Hot exit diameter	11 mm
Cold exit area	30.3 mm^2
Cold exit diameter	6.2 mm
Nozzle inlet area	8.2 mm^2
Nozzle width	1.41 mm
Working tube length	106 mm

shown in fig. 4. Finer mesh was considered near the outlets, inlet, and walls. It can be seen that there is not much demerit in reducing the average cell volume size below 0.045 m^2 (25,000 cells) and 0.0145 m^3 (200,000 cells), for 2-D and 3-D simulations, respectively.

Boundary conditions

In the CFD model the cold outlet boundary assumed pressure outlet. The inlet is modeled as a mass flow inlet where the total mass flow rate and inlet temperature were fixed at 8.35 g/s and 297 K, respectively. The cold exit and inlet static pressure were specified according to experimental measurements. The hot outlet also assumed as pressure outlet boundary. The hot exit static pressure is adjusted in a way to vary the cold mass fraction. No slip, adiabatic boundary was considered for tube walls.

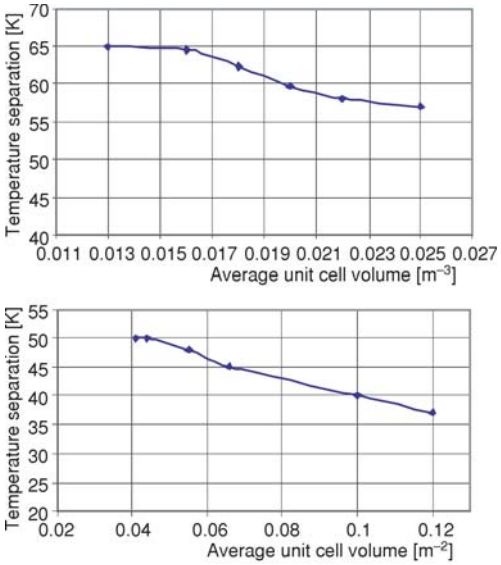

Figure 4. Grid independence study on temperature separation

Governing equation

For 2-D compressible flow, the conservation of mass, momentum and the state equation can be written as:

$$\frac{\partial}{\partial x_i}(\overline{\rho}\widetilde{u}_i) = 0 \tag{1}$$

$$\frac{\partial}{\partial x_j}(\overline{\rho}\widetilde{u}_i\widetilde{u}_j) = -\frac{\partial P}{\partial x_i} + \frac{\partial}{\partial x_j}[\bar{t}_{ji} - \overline{\rho u_j'' u_i''}] \tag{2}$$

$$P = \overline{\rho}\mathrm{R}\widetilde{T} \tag{3}$$

Turbulence models

k-ε standard turbulence model

For *k-ε* model, the turbulence kinetic energy *k* and the dissipation rate *ε*, with eqs. (1-3) are solved numerically by a control volume method. The *k* and *ε* equation can be written as:

$$\rho\frac{Dk}{Dt} = \frac{\partial}{\partial x_i}\left[\left(\mu + \frac{\mu_\mathrm{t}}{\sigma_\mathrm{k}}\right)\frac{\partial k}{\partial x_i}\right] + G - \rho\varepsilon \tag{4}$$

$$\rho\frac{D\varepsilon}{Dt} = \frac{\partial}{\partial x_i}\left[\left(\mu + \frac{\mu_\mathrm{t}}{\sigma_\mathrm{k}}\right)\frac{\partial \varepsilon}{\partial x_j}\right] + C_{1\varepsilon}\frac{\varepsilon}{k}G - C_{2\varepsilon}\rho\frac{\varepsilon^2}{k} \tag{5}$$

In eqs. (4) and (5), *G* is the kinetic energy generation of turbulence kinetic energy term and σ_k – the turbulence Prandtl number. In compressible case, *ε* term will be divided into two terms: solenoidal dissipation rate of *k*, ε_s and dilation dissipation rate of *k*, ε_d:

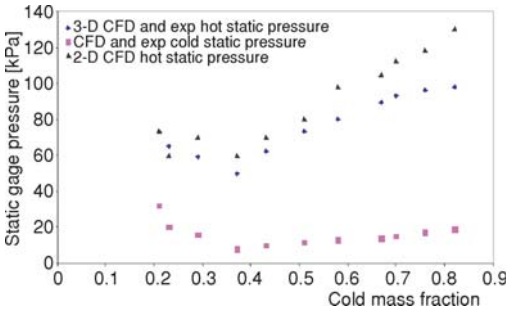

Figure 5. CFD model predictions of hot and cold exit static pressure as a function of the cold fraction

$$\varepsilon = \varepsilon_{\mathrm{s}} + \varepsilon_{\mathrm{d}} \tag{6}$$

In eq. (5) $C_{1\varepsilon} = 1.44$, $C_{2\varepsilon} = 1.92$, σ_{ε} is turbulent Prandtl number. μ_{t} is computed by $\mu_{\mathrm{t}} = \rho C_{\mu} k^2/\varepsilon$, where $C_{\mu} = 0.09$.

RNG k-ε turbulence model

The RNG k-ε model was also investigated in this paper. This model is based on Renormalized group theory. The difference between this model and k-ε is that this model accounts the effect of swirl on turbulent intensity. The k-ε equations can be written as:

$$\rho \frac{Dk}{Dt} = \frac{\partial}{\partial x_j}\left[\alpha_{\mathrm{k}} \mu_{\mathrm{eff}} \frac{\partial k}{\partial x_j}\right] + G - \rho\varepsilon \tag{7}$$

$$\rho \frac{D\varepsilon}{Dt} = \frac{\partial}{\partial x_j}\left[\alpha_{\varepsilon} \mu_{\mathrm{eff}} \frac{\partial \varepsilon}{\partial x_j}\right] + C_{1\varepsilon}\frac{\varepsilon}{k} G - C_{2\varepsilon}\rho\frac{\varepsilon^2}{k} \tag{8}$$

where $C_{\varepsilon 1}$ and $C_{\varepsilon 2}$ are coefficients given as 1.45 and 1.83. α_{k} and α_{ε} are inverse effective Prandtl numbers of k and ε. The differential equation for turbulent viscosity is:

$$\mathrm{d}\left(\frac{\rho^2 k}{\sqrt{\varepsilon\mu}}\right) = 1.72 \frac{\dfrac{\mu_{\mathrm{eff}}}{\mu}}{\sqrt{\left(\dfrac{\mu_{\mathrm{eff}}}{\mu}\right) - 1 + C_v}} \mathrm{d}\left(\frac{\mu_{\mathrm{eff}}}{\mu}\right) \tag{9}$$

SST k-ω turbulence model

The SST k-ω was developed to accurate formulation of the k-ω in the near wall regions. To achieve this, the k-ε model is converted into a k-ω formulation which gives:

$$\frac{D(\rho k)}{Dt} = \frac{\partial}{\partial x_i}\left[\Gamma_{\mathrm{k}} \frac{\partial k}{\partial x_j}\right] + G_{\mathrm{k}} - Y_{\mathrm{k}} \tag{10}$$

$$\frac{D(\rho\omega)}{Dt} = \frac{\partial}{\partial x_j}\left[\Gamma_{\omega} \frac{\partial \omega}{\partial x_j}\right] + G_{\omega} - Y_{\omega} + D_{\omega} \tag{11}$$

where G represents the generation of turbulence kinetic energy, Y_{k} and Y_{ω} represents the generation of k and ω and D_{ω} represents the cross diffusion term.

$$\mu_{\mathrm{t}} = \rho \frac{k}{\omega} \frac{1}{\max\left[\dfrac{1}{\alpha^*}, \dfrac{\Omega F_2}{\alpha_1 \omega}\right]} \tag{12}$$

The Ω is the mean rate of rotation and F_2 is the blending function, and α^* is given by:

$$\alpha^* = \alpha^* \left(\alpha_0^* + \frac{\frac{\mathrm{Re}_t}{R_k}}{1 + \frac{\mathrm{Re}_t}{R_k}} \right) \tag{13}$$

where $\mathrm{Re}_t = \rho k/m\omega$, $R_k = 6.0$ and, $\alpha_0^* = 0.024$

Results

In the CFD models, the cold exit static pressures were specified at experimental data and the hot exit pressure changes until the right cold fraction is obtained. Figure 2 shows that the values of the hot exit static pressures are higher than experimental results. These values are the same for three turbulence models. However, in 3-D model these pressures are the same with experimental results. This difference accounts for circumferential assumption of inlet nozzles. Thus, the hot outlet pressure was imposed at a higher value than experiment to reach acceptable cold mass fraction in 2-D model. The temperature separation obtained in this paper was compared with the experimental results of Skye *et al*. [16].

As fig. 6 shows, the cold temperature separation for three turbulence models is close to the result of Skye. Like Skye's results, all three turbulence models under predicted the cold exit temperature difference, but the curves show the trend falls into good agreement with the experimental results and 3-D simulation model. At a cold mass fraction of approximately 0.37, the peak values recorded for cold temperature separation are between 30-32 °C. Results obtained using RNG *k-ω* and SST *k-ω* turbulence models are closer to experimental results.

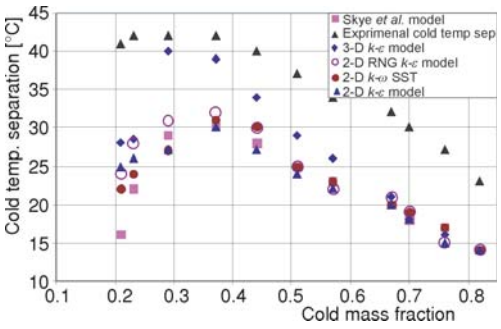

Figure 6. Cold exit temperature difference as a function of cold mass fraction

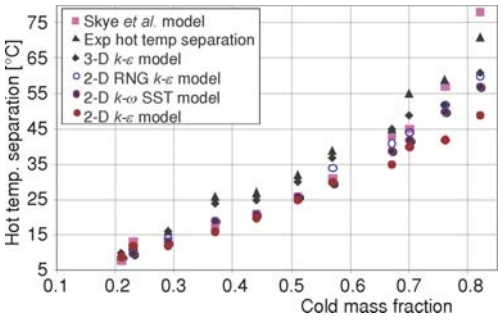

Figure 7. Hot exit temperature difference as a function of cold mass fraction

Figure 7 shows the hot exit temperature separation for three turbulence models. It is seen that among these models, the RNG model is closer to the experimental results. The three turbulence models follow similar pattern with no significant difference up to cold fraction 0.58. The hot exit temperature difference between RNG and *k-ε* is about 5-10 °C and the results of SST *k-ω* and RNG are the same except for the last two cold fractions. The difference between hot exit temperature separation and experimental results is nearly 2-10 °C.

To ensure better results, performance of vortex tube should be determined by the rate of energy separation which can be calculated by:

$$Q_{\mathrm{h}} = m_{\mathrm{k}} c_{\mathrm{p}} (T_{\mathrm{h}} - T_{\mathrm{in}}) \tag{14}$$

$$Q_{\mathrm{c}} = m_{\mathrm{c}} c_{\mathrm{p}} (T_{\mathrm{in}} - T_{\mathrm{c}}) \tag{15}$$

In the absence of heat loss or heat gain, values of Q_{h} and Q_{c} should be equal. Figure 8 shows the power separation for three turbulence models. Although the results are less than experimental ones, the trends and variation by RNG and *k-ω* model are in good agreement with the experimental results.

The cold and hot power separations in RNG model are close to each other compared to the other models. All three models show maximum power separation with a cold mass fraction at 0.65.

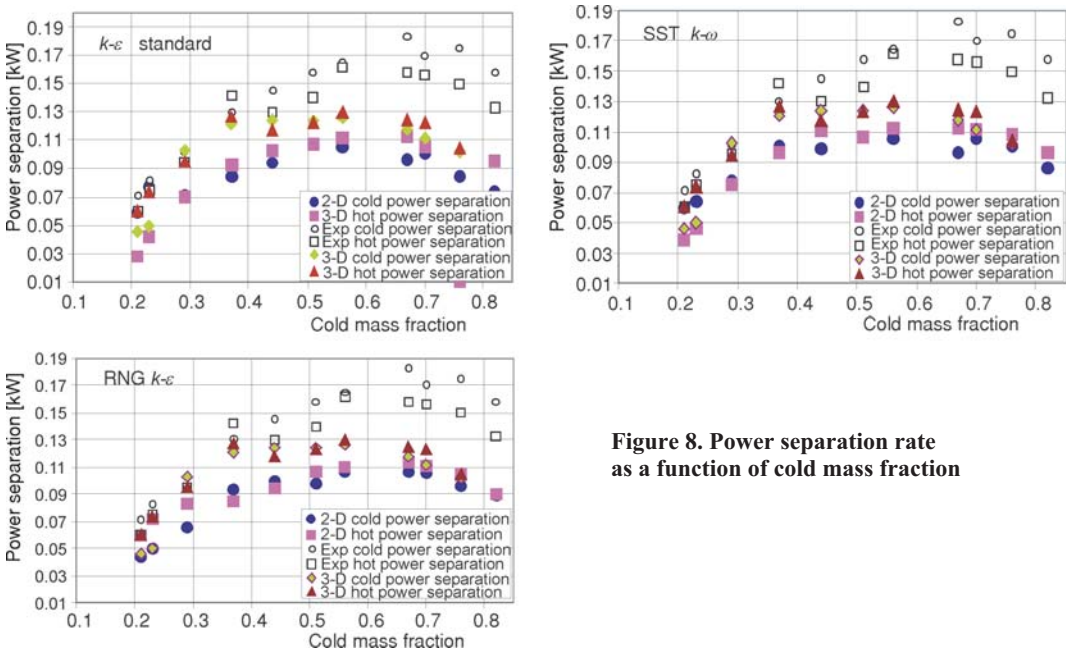

Figure 8. Power separation rate as a function of cold mass fraction

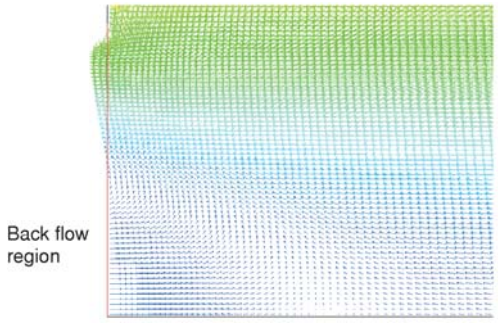

Figure 9. Reverse flow on low cold mass fractions

Before cold mass fraction 0.31, the pressure on the cold outlet is more than the inner pressure near the axis. This pressure leads to reversing flow phenomena which causes the cold outlet to become hotter by heat transfer to the tube as also mentioned by Skye *et al*. [16] (fig. 9). For all turbulence models this phenomenon is the reason for poor energy conservation at low cold mass fractions. On the other hand, the heat loss to the tube wall accounts for energy separation differences of experiments at high cold mass fractions.

The velocity field

Figure 10 shows the radial profile of the axial velocity at different axial locations (z = = 0.025, z = 0.050, z = 0.075 m) for cold mass fraction 0.37. It is seen that, the axial velocity of turbulence models are different at the cold exit. The difference in axial velocities is nearly 5-10 m/s and decreases by increasing the axial distance. The maximum axial velocity is near the tube wall. The flow reversal takes place at about 3 mm from the center of tube. The direction of flow from axis to this point is toward the cold exit and the rest of the flow has a positive direction to the hot exit.

Figure 11 illustrates the radial profiles for the swirl velocity at different axial locations. A comparison of the swirl velocities reveals that the k-ω model predicts higher velocity than RNG and k-ε model. The difference between swirl velocities increases as approaching the hot exit. Free vortex or potential vortex regime ($V \propto 1/r$) is formed in small regions near the wall. The magnitude of the swirl velocity decreases near the hot exit.

The radial velocity is shown in fig. 12 for three axial positions. The difference between radial velocities for turbulence model is negligible. A comparison of velocity components shows that the magnitude of swirl velocity is much greater than of axial or radial velocities;

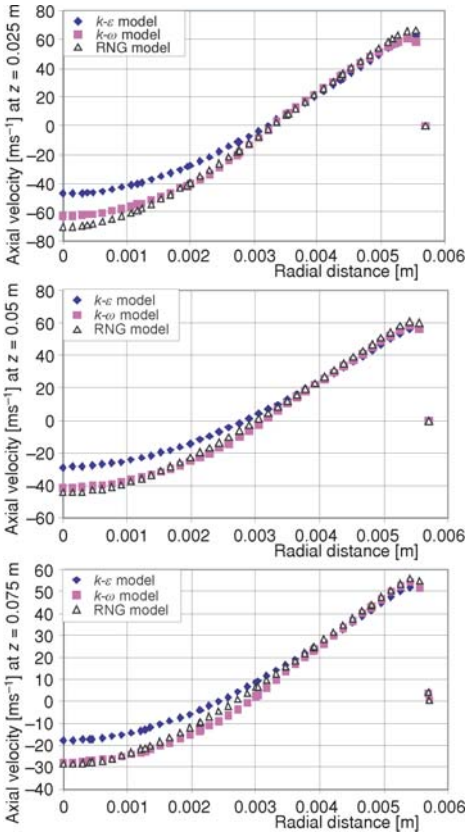

Figure 10. Radial profiles of axial velocity V_z, at three different axial positions

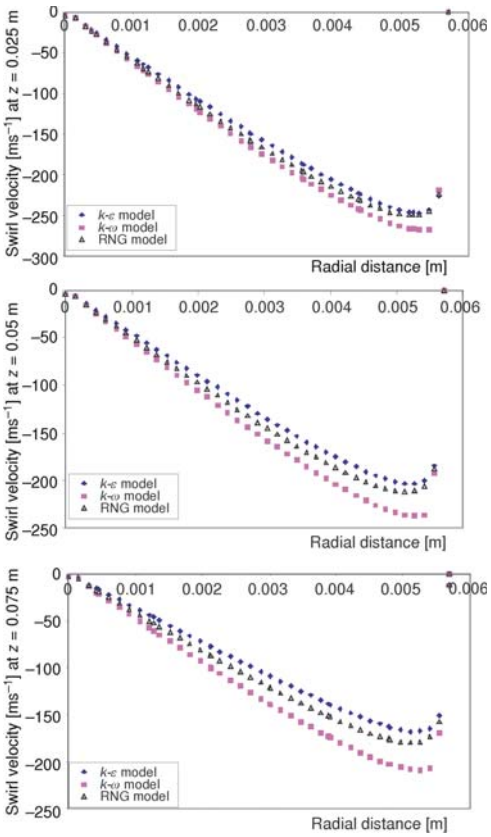

Figure 11. Radial profiles of swirl velocity V_θ, at three axial positions

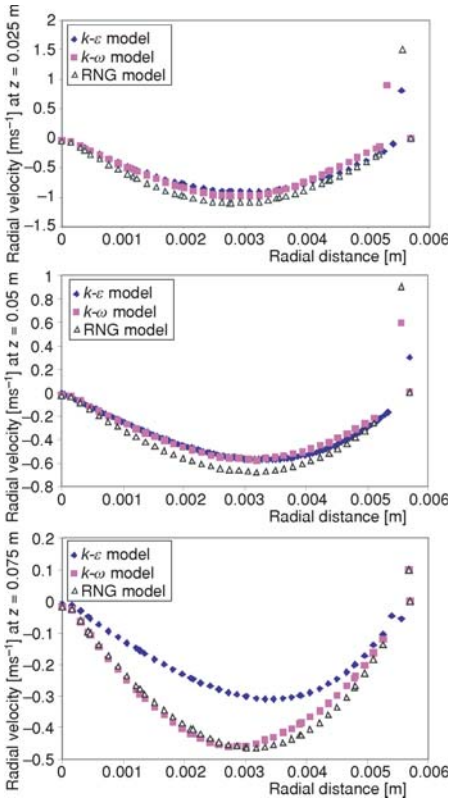

Figure 12. Radial profiles of radial velocity V_z at three axial positions

therefore, the swirl velocity plays an important role in separation of energy or temperature.

The temperature field

Figures 13 and 14 illustrate the contours of total temperature and radial profiles of total and static temperature for the three turbulence models. Considering the same location, the total and static temperature of k-ε model have higher values for z = 0.025m than RNG and k-ω which explains lower cold temperature separation of k-ε model. On the other hand, at z = 0.095 m the RNG model has higher values among others and this difference outstands for the cold mass fraction range 0.67-0.82 which describes higher hot temperature separation with this model.

Figure 13. Contours of total temperature (a) k-ε, (b) RNG, and (c) SST k-ω

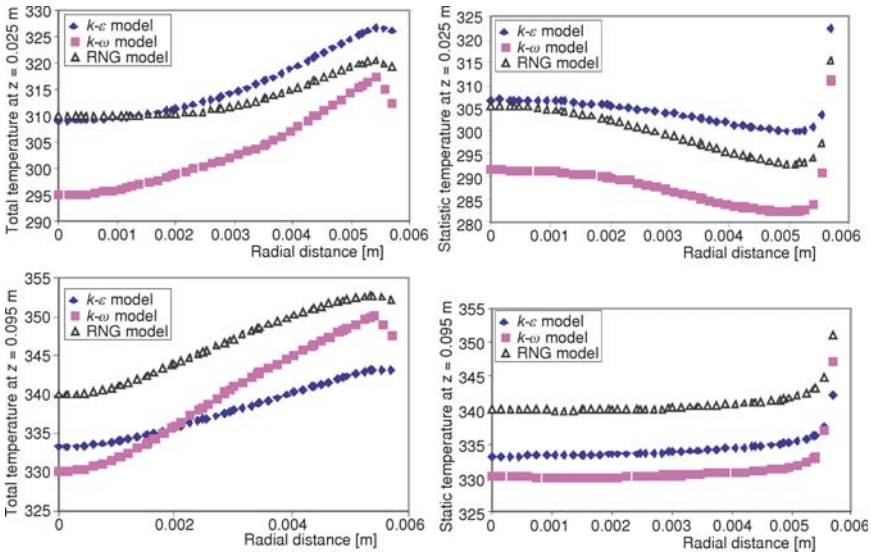

Figure 14. Radial profiles of static and total temperature at two axial positions

The difference between shape and profile of total and static temperature is due to the swirl velocity. The SST k-ω and RNG model have higher swirl velocity than k-ε. It is seen that in SST model the cold region expands more than k-ε and RNG model and the hot region concentrates near the hot end. Although SST k-ω model has higher values of swirl velocity, RNG model provide a better prediction of hot temperature than this model.

The radial profiles of total temperature show that the maximum total temperature is near periphery and the total temperature increases by adding to axial distance. Figure 15 shows the contour of static temperature for the cold mass fraction 0.37 and 0.81 for the K-ε model. By increasing the cold mass fraction the hot region expands and the cold region compresses.

The pressure field

Variations of static pressure in three radial sections are plotted in fig. 16. A closer look reveals that the pressures of the particles vary similar to that of velocity as it moves to the hot and cold outlet. Most of the expansion occurs within the inlet nozzle, causing considerable amount of swirl velocity but the static pressure doses not change much along the tube up to the hot end. On the other hand, the difference of pressure near the axis along the axial direction is considerable. The drag force caused by the difference of pressure between the flow field and cold end exit will act on particles moving toward the cold end with high axial velocity so the turbulence models show more axial velocity variation in the reverse flow whereas they show more variation in swirl velocity near the tube wall.

Conclusions

A numerical computation model being steady, axisymmetric with swirl has been done to predict the flow field and temperature in a standard vortex tube with three turbulence models.

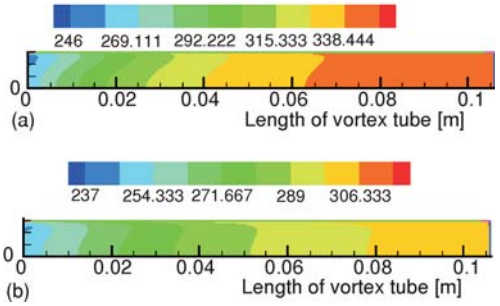

Figure 15. Contours of static temperature (a) for cold mass fraction 0.82, (b) for cold mass fraction 0.37 for 2-D k-ε model

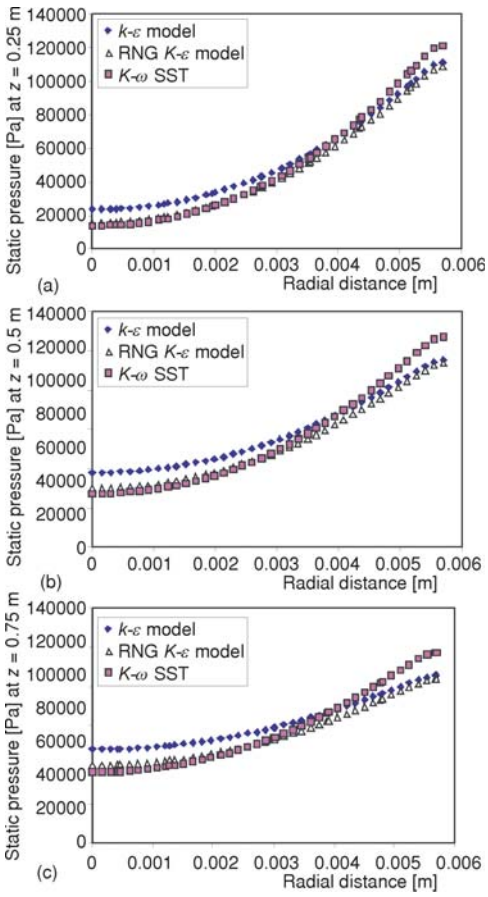

Figure 16. Radial profiles of Static Pressures at three different axial positions

Simulations were conducted for different cold mass fractions and due to large discrepancies between 2-D and experimental results of Skye, validation in the 3-D model is also considered.

Among these models, the result of RNG k-ε model is closer to experimental results. The results of SST k-ω are so close to the RNG model except for the last two cold mass fractions.

The profiles of axial, radial and swirl velocities show that the magnitude of swirl velocity is significantly greater than others so that the swirl velocity plays an important role in energy separation.

Contours of the total temperature and radial profiles of total and static temperature are different in each model. In the SST k-ω model the cold region expands and the hot region concentrates near the hot end compared to the others.

By increasing the cold mass fraction the hot region expands and the cold region compresses.

The drag forced caused by the difference of pressure will act of particles to move toward cold and hot ends. The difference between turbulence models for static pressure happens near the tube wall and the axis. Therefore, variation of swirl and axial velocity happen in these regions.

Nomenclature

C_p – specific heat capacity, [Jkg^{-1}k^{-1}]
D – diameter of vortex tube, [mm]
k – turbulence kinetic energy, [m^2 s^{-2}]
k_{eff} – effective thermal conductivity, [Wm^{-1}K^{-1}]
L – length, [mm]
l_{h} – width of hot exit, [mm]
$\dot{m}$ – mass flow rate, [kgs^{-1}]
P – pressure, [Pa]
R – ideal gas constant, [Jkg^{-1}K^{-1}]
r, z, θ – components of cylindrical co-ordinate system, [m]
r – radial distance from axis, [mm]
T – temperature, [K]
V – velocity, [ms^{-1}]
V_{n} – total velocity vector, [ms^{-1}]
V_θ – tangential velocity, [ms^{-1}]
V_{r} – radial velocity, [ms^{-1}]
V_{z} – axial velocity, [ms^{-1}]

Greek symbols

ε – turbulent dissipation rate, [m^2 s^{-1}]
μ – dynamic viscosity, [kgm^{-1}s^{-1}]
μ_{t} – turbulent viscosity, [kg m^{-1}s^{-1}]
ξ – mass flow fraction
ρ – density, [kg m^{-3}]
σ – stress, [Nm^{-2}]
τ – shear stress, [N m^{-2}]

Subscripts

i – inlet gas
c – cold gas
h – hot gas

References

[1] Aronson, R. B., Vortex Tube Cooling with Compressed Air, *Journal of Machine Design., 48* (1976), 28, pp. 140-143
[2] Ranque, G. J, Experiences on Expansion in a Vortex with Simultaneous Exhaust of Hot Air and Cold Air (in French), *Journal of Phys.Radium, 4* (1933), 7, pp. 112-114
[3] Hilsch, R., The Use of Expansion of Gases in a Centrifugal Field as a Cooling Process (in German), *Z. Naturforschung, 1* (1946), Feb., pp. 208-214
[4] Fulton, C. D., Comments on the Vortex Tube, *Journal of ASRE Refrigeration Engineering, 59* (1951), 1, pp. 984
[5] Kassner, R, Knoernschild, E, Friction Laws and Energy Transfer in Circular Flow, Wright-Patterson Air Force basr. Technical Report, 1948, F-TR-2198ND OH
[6] Scheper, G. W., The Vortex Tube Internal Flow Data and a Heat Transfer Theory, *Journal of ASRE Refrigeration Engineering, 59* (1951), Oct., pp. 985-989

[7] Ahlborn, B., Gordon, J., The Vortex as Classical Thermodynamic Refrigeration Cycle, *Journal of Applied Physics., 88* (2000), 6, pp. 3645-3653
[8] Stephan, K., *et al*., An Investigation of Energy Separation in a Vortex Tube, *International Journal of Heat and Mass Transfer, 26* (1983), 3, pp. 341-348
[9] Gutsol, A. F., The Ranque Effect, *Journal of Physics, Uspekhi, 40* (1997), 6, pp. 639-658
[10] Kurosaka, M., Acoustic Streaming in Swirling Flows, *Journal of Fluid Mechnics, 124* (1982), Nov., pp. 139-172
[11] Frohlingsdorf, W., Unger, H., Numerical Investigation of the Compressible Flow and the Energy Separation in the Ranque-Hilsch Vortex Tube, *International Journal of Heat and Mass Transfer, 42* (1999), 3, pp. 415-422
[12] Bruun, H. H., Experimental Investigation of the Energy Separation in Vortex Tubes, *Journal of Mechanical Engineering Science, 11* (1969), 6, pp. 567-582
[13] Promvonge, P., Numerical Simulation of Turbulent Compressible Vortex-Tubes Flow, *Proceedings on CD,* Third ASME/JSME *Joint Fluid Engineering*, Conference San Francisco, Cal., USA, 1999
[14] Behera, U., *et al*., CFD Analysis and Experimental Investigation Towards Optimizing the Parameter of Ranque-Hilsch Vortex Tube, *International Journal of Heat and Mass Transfer, 48* (2005), 10, pp. 1961-1973
[15] Aljuwayhel, N. F., *et al*., Parametric and Internal Study of the Vortex Tube Using a CFD Model, *International Journal of Refrigeration,28* (2005), 3, pp. 442-450
[16] Skye, H. M., *et al*., Comparison of CFD Analysis to Empirical Data in a Commercial Vortex Tube, *International Journal of Refrigeration, 29* (2006), 1, pp. 71-80
[17] Sohn, C.-H., *et al*., Experimental and Numerical Studies in a Vortex Tube, *Journal of Mechanical Science and Technology, 20* (2006), 3, pp. 418-425
[18] Xue, Y., *et al*., A Critical Review of Temperature Separation in a Vortex Tube, *Journal of Experimental Thermal and Fluid Science, 34* (2010), 8, pp. 1367-1374
[19] Akbesme, S., *et al*., Numerical Study of Temperature Separation in a Rangue-Hilsch Vortex Tube, *American Journal of Engineering and Applied Science, 1* (2008), 3, pp.181-187
[20] Kirmaci, V., Optimization of Counter flow Ranque-Hilsch Vortex Tube Performance Using Taguchi Method, *International Journal of Refrigeration, 32* (2009), 7, pp. 1487-1494
[21] Hossein Nezhad, A., Shamsoddini, R., Numerical Three-Dimensional Analysis of the Mechanism of Flow and Heat Transfer in a Vortex Tube, *Thermal Science, 13* (2009), 4, pp. 183-196
[22] Bramo, A. R., Pourmahmoud, N., Computational Fluid Dynamics Simulation of Length to Diameter Ratio Effect on the Energy Separation in a Vortex Tube, *Thermal Science, 15* (2011), 3, pp. 833-848
[23] Farouk, T., Farouk, B., Large Eddy Simulations of the Flow Field and Temperature Separation in the Ranque-Hilsch Vortex Tube, *International Journal of Heat and Mass Transfer, 50* (2007), 23-24, pp. 4724-4735
[24] Dutta, T., *et al*., Comparison of Different Turbulence Models in Predicting the Temperature Separation in a Ranque- Hilsch Vortex Tube, *International Journal of Refrigeration, 33* (2010), 4, pp. 783-792

Paper submitted: July 27, 2011
Paper revised: February 13, 2012
Paper accepted: October 24, 2012